Available online at www.sciencedirect.com
SCIENCE DIRECT®
Physica B 362 (2005) 145–152
PHYSICA B
www.elsevier.com/locate/physb

EXAFS determination of Hf localization in HDDR–Nd–Fe–B–Hf alloys

C.E. Rodríguez Torres*, M.B. Fernández van Raap, F.H Sánchez, A.F. Pasquevich

Departamento de Física, Facultad de Ciencias Exactas, IFLP, Universidad Nacional de La Plata, 49 y 115 CC 67, 1900 La Plata, Argentina

Received 4 February 2005; accepted 4 February 2005

Abstract

The local structure around Hf in $Nd_{15.78}Fe_{76.3-x}Hf_xB_{7.8}$ ($x = 0.1$ and 0.2) submitted to conventional and solid hydrogenation–disproportionation–desorption–recombination (HDDR) sequence was studied by extended X-ray absorption fine structure (EXAFS) in order to understand the relation between the presence of Hf and magnetic anisotropy found only in solid-HDDR samples. EXAFS results show that Hf is not in the $Nd_2Fe_{14}B$ structure but incorporated into a local atomic arrangement (HfB ClNa-type) which is the same for as-cast, solid and conventional HDDR samples. It is concluded that the magnetic anisotropy induced by Hf addition to NdFeB alloys must be related to microstructural features.

PACS: 61.10.Ht; 75.50.Bb; 75.60.Ej; 75.30.Gw

Keywords: XAFs; $Nd_2Fe_{14}B$; Magnetic anisotropy; HDDR

1. Introduction

It is known that additives such as Zr, Ga, and Hf improve the magnetic properties of Nd–Fe–B powders produced by the hydrogenation, disproportionation, desorption and recombination (HDDR) sequence, as a result of inducing the magnetic anisotropy [1]. Best properties were obtained for addition of 0.2 at% of Zr or Hf, and 1 at% of Ga. For larger additive concentrations the magnetic properties deteriorate [2]. The origin of the anisotropy was suggested to be from the undecomposed $Nd_2Fe_{14}B$ grains which induce a preferential crystallographic orientation of the newly formed grains [3,4]. Despite the extensive effort, the mechanism of inducement of magnetic

*Corresponding author. Tel.: +54 2214246062; fax: +54 221252006.
E-mail address: torres@fisica.unlp.edu.ar (C.E.R. Torres).

0921-4526/$ - see front matter © 2005 Elsevier B.V. All rights reserved.
doi:10.1016/j.physb.2005.02.004

anisotropy, especially the role of additives is not well understood. Extended X-ray absorption fine structure (EXAFS) constitutes an appropriate tool to obtain information on local additives environment. Chemical or microstructural features related to low concentration additives are not easily detected by other techniques. Many EXAFS experiments at Zr K-edge on Zr-added Nd–Fe–B alloys have been reported. These results seem to be highly dependent on sample preparation method and alloy composition. For 0.5 at% of Zr as-cast alloys, some authors have reported that Zr does not segregate and preferentially occupies the Fe(j_1) and Fe(j_2) sites of the $Nd_2Fe_{14}B$ structure [5], suggesting that Zr in j_2 sites stabilizes this phase, leaving part of the original grains undisproportionated. These grains would then serve as a seed for grain growth during the recombination step. Other authors have reported that Zr addition (0.7–2 at%) results in the formation of ZrB_2 phase [6] in as cast samples homogenized at 1000 °C. For a melt-spun $(Nd_{0.8}Zr_{0.2})_2$ $Fe_{14}B$ (2.35 at%) it was found that Zr occupies the Nd sites [7]. Unfortunately, experiments for samples with Zr content lower than 0.2 at% (optimal Zr concentration for best magnetic properties) have not been reported. To our knowledge no previous EXAFS was performed at Hf L_{III}-edge.

In order to contribute to the understanding of mechanism inducing or improving magnetic anisotropy in Hf-added Nd–Fe–B alloys, we report here a study using EXAFS on Hf L_{III}-edge in anisotropic and isotropic $Nd_{15.8}Fe_{76.3-x}Hf_xB_{7.9}$ ($x = 0.1,\ 0.2$) samples obtained from different HDDR cycles. The samples were also structurally characterized by X-ray diffraction (XRD), ^{57}Fe Mössbauer effect spectroscopy (ME), and were magnetically characterized using vibrating sample magnetometry (VSM).

2. Experimental details

Commercially available ingot alloys with nominal composition $Nd_{15}Fe_{77}B_8$ were arc melted with Nd, Fe, and Hf to give $Nd_{15.78}Fe_{76.3-x}Hf_xB_{7.8}$ ($x = 0.1$ and 0.2), homogenized for 67 hours at 1050 °C under vacuum, and then crushed into a fine powder (less than 150 μm). These alloys (500 mg) were used to perform hydrogenation–disproportionation (HD) experiments, followed by desorption–recombination (DR) ones.

Two types of HD experiments were performed: S-HD (solid HD) and C-HD (conventional HD). In the first case, the powders were heated in vacuum to temperatures of 800, 850 or 900 °C, and then hydrogen was supplied at a constant pressure of 0.95 bar for 100 min. In the second one the hydrogen supply was performed at RT and then, after 1 h, the samples were heated at 800, 850 or 900 °C for 100 min under a constant H_2 pressure of 0.95 bar.

The recombination reaction was always carried out at 850 °C and in order to promote a slow transformation the hydrogen pressure was lowered only to 0.1 bar. The powder was held under these conditions for 30 min, followed by a final desorption stage of 5 min under continuous pumping and then was rapidly cooled to RT. Similar procedures were performed on $Nd_{16}Fe_{76}B_8$ samples in order to compare the effect of Hf on the magnetic behaviour.

The X-ray absorption experiments at the Hf L_{III} edge (9561 eV) were performed at XAS1 beam line of LNLS (Campinas, Brazil) using a Si (1 1 1) channel-cut crystal monocrhromator. The data were collected in the fluorescence mode using a Ge 15-elements solid state detector.

$k\chi(k)$ oscillations were extracted using Winxas program [8]. A linear pre-edge background was subtracted and the spectra were normalized to the height of the absorption edge. The $k\chi(k)$ EXAFS signal was Fourier-transformed within a Bessel window between 3.1 and 10 $Å^{-1}$. Ab initio calculations of the oscillations were also performed with FEFF7 code [9].

^{57}Fe Mössbauer effect (ME) measurements were performed under transmission geometry with a standard constant acceleration spectrometer holding a ^{57}Co*Rh* radioactive source.

XRD was performed using Cu Kα radiation with a Phillips X-ray diffractometer on crushed samples (powder size less than 0.125 mm).

Magnetic properties were determined by VSM at room temperature with a maximum applied field of 8 T. Prior to the VSM measurements the

powders were cold compacted to a disk form under a magnetic field of 2 T placed in a direction perpendicular to the disk axis.

In order to quantify the magnetic parameters (saturation polarization J_s, intrinsic coercivity h_c and remanent polarization J_r) for each sample, we propose the following fitting function for the demagnetization data

$$J = J_s\left[g\frac{2}{\pi}\tan^{-1}\left[\left(\frac{H+h_c}{h_c}\right)\tan\left(\frac{\pi S}{2}\right)\right] + (1-g)\tanh(aH)\right], \quad (1)$$

where S is equal to J_r/gJ_s and a is constant. The first term in the formula is commonly used for materials where the anisotropy field is much lower than the maximum external field [10]. In the present case, as magnetocrystalline anisotropy is huge and the grains are randomly or partially randomly oriented, the maximum applied field (8 T) is insufficient to reach saturation and a second term is needed to take into account the high field susceptibility behaviour. In this term, $(1-g)$ gives the fraction of grains, which do not have their ease axes in the field direction. Systematically, the g-fitted values for the demagnetization curve with the external field in the e-direction are the complements of the one fitted for the same sample with the external field in the h-direction, indicating consistency.

It is well known that for an $Nd_2Fe_{14}B$ single-crystal a field of 1 T applied in the [0 0 1] is enough to achieve magnetic saturation, while when the field is applied in a [1 1 0] or [1 0 0] more than 12 T are needed [11]. The saturation polarization was fixed to the single crystal value.

Due to the fact that some of our demagnetization curves show an inflexion feature (and consistently the magnetic susceptibility $\chi = dJ/dH$ has two maxima) two J components are needed,

$$J = f_1J_1 + f_2J_2 \quad (2)$$

with $f_1 + f_2 = 1$ and the remanent polarizations $J_{r1,2}$ are obtained from fitted values as $J_{r1} = f_1gS$ and $J_{r2} = f_2gS$.

The fitting function we proposed here for demagnetisation curves allows us to deconvolute the two magnetic components, estimate their fractions f_1 and f_2, the values of h_c, J_r of each component and the fraction (g) of grains which have their ease axes in the e-direction. The g values for each component were restricted to be equal, because although relaxing this restriction the goodness of the fit increases keeping the g values nearly equal, the correlation between parameters of same kind is too high.

3. Results

The hysteresis loops, for easy (e, in the plane of the disk) and hard (h, perpendicular to the plane of the disk) magnetization directions are shown in Fig. 1 for all the alloys S-HDDR processed at 850 °C. For the ternary alloy the loop is almost the same for both e and h directions, which is characteristic of randomly, oriented grains of a

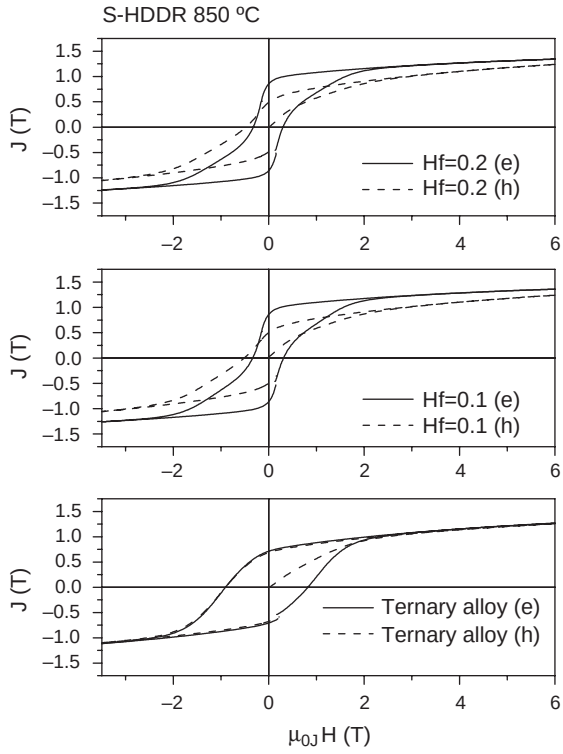

Fig. 1. Hysteresis loops of $Nd_{15.78}Fe_{76.3-x}Hf_{0.2}B_{7.8}$ ($x = 0.1$ and 0.2) and $Nd_{16}Fe_{76}B_8$ submitted to S-HDDR at 850 °C.

single magnetic component sample, i.e. of an isotropic material. The fit of these loops using formula (1) leads to a remanent polarization of $J_r = 0.71\,T$, intrinsic coercivity of $\mu_{0J}H_c = 0.91\,T$, and g value of 0.5, for both directions. For non-oriented samples $g = 1/3$ is expected. The present value indicates that the samples were partially oriented during compaction under a magnetic field.

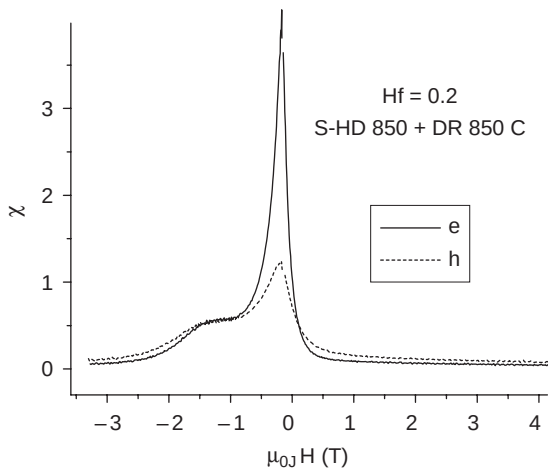

Fig. 2. Susceptibility (e and h directions) curves of Hf ($x = 0.2$) added sample submitted to S-HDDR 850 °C.

For the Hf-doped alloys (S-HDDR 850 °C) strong anisotropy is observed. The remanence is 79% higher for the e-direction and coercivity 0.57% lower. In this case the pattern reminds us the one expected for the overlapping loops originated from two magnetic phases with different coercivities. Fig. 2 shows the susceptibility (e and h directions) curves for Hf-added sample S-HDDR treated at 850 °C (obtained by differentiating curves of Fig. 1). It has two maxima confirming the presence of two magnetic components. As it can be seen the high coercivity one is isotropic while the other one is highly anisotropic. The fit of the demagnetization curves with two components (Formula (2)) allows us to determine remanence and coercivity of both components; fitted values are listed in Table 1. The g value is 38% higher for the e-direction than for the h-direction.

Fig. 3a shows the hysteresis loops (e-direction) of Hf added (0.2) sample submitted to S- and C-HDDR treatments at 800, 850 and 900 °C, it can be seen that the reactions lead to almost isotropic, single phase-like loops, except for samples S-HDDR treated at 800 and 850 °C. However, from the corresponding susceptibility graph for S-HDDR samples also two contributions appear for the sample treated at 900 °C (see small bump at 0.78 T in Fig. 3b). The results obtained from the

Table 1
Fitted values, using formulas (1) or (2), of magnetic properties of $Nd_{16}Fe_{76}B_8$ and $Nd_{15.78}Fe_{76.3-x}Hf_xB_{7.8}$ ($x = 0.1$ and 0.2)

Sample	Treatment	h_{c1} (T)	h_{c2} (T)	J_{r1} (T)	J_{r2} (T)	f_1	g	a
$Nd_{16}Fe_{76}B_8$ (e)	S-HD 850 °C + DR	—	0.934_2	—	0.706_3	—	0.534_2	0.0649_7
$Nd_{16}Fe_{76}B_8$ (h)	S-HD 850 °C + DR	—	0.939_3	—	0.681_3	—	0.520_2	0.0661_6
$x = 0.1$ (e)	S-HD 850 °C + DR	0.226_2	1.154_9	0.486_3	0.334_1	0.646_5	0.637_1	0.0505_5
$x = 0.1$ (h)	S-HD 850 °C + DR	0.3378_5	1.419_8	0.269_2	0.212_1	0.714_6	0.460_1	0.0735_3
$x = 0.2$ (e)	S-HD 800 °C + DR	0.329_3	1.385_3	0.299_2	0.470_2	0.509_4	0.580_1	0.0575_3
$x = 0.2$ (h)	S-HD 800 °C + DR	0.43_1	1.443_4	0.212_3	0.387_2	0.526_9	0.492_2	0.069_3
$x = 0.2$ (e)	S-HD 850 °C + DR	0.229_1	1.168_1	0.500_2	0.316_2	0.655_5	0.624_1	0.050_6
$x = 0.2$ (h)	S-HD 850 °C + DR	0.323_4	1.465_9	0.267_1	0.202_2	0.726_6	0.454_2	0.0745_3
$x = 0.2$ (e)	S-HD 900 °C + DR	0.74_3	1.334_4	0.210_1	0.578_2	0.321_3	0.501_2	0.069_6
$x = 0.2$ (h)	S-HD 900 °C + DR	0.79_4	1.351_5	0.219_1	0.523_2	0.364_3	0.485_3	0.072_8
$x = 0.2$ (e)	C-HD 900 °C + DR	—	1.300_2	—	0.779_2	—	0.471_2	0.0795_6
$x = 0.2$ (h)	C-HD 900 °C + DR	—	1.297_2	—	0.779_2	—	0.464_2	0.0784_6

The hydrogenation/disproportionation (HD) treatment temperature is listed in second column, always the desorption/recombination (DR) temperature was 850 °C. $h_{c1,2} = \mu_{0J}H_c$ stand for intrinsic coercivity and $J_{r1,2}$ for remanent polarization.

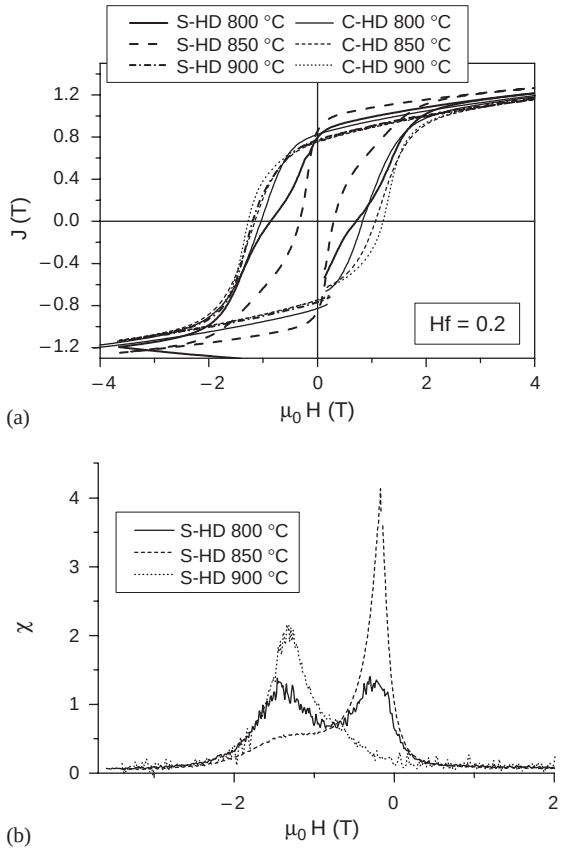

Fig. 3. (a) Comparison of hysteresis curves (applied field in the *e*-direction) for various solid and conventional HDDR processed Hf ($x = 0.2$) added samples, at the indicated HD temperatures. (b) Susceptibility for the S-HDDR processed samples of (a).

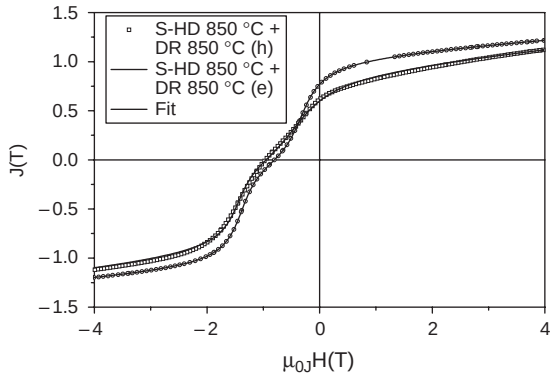

Fig. 4. Demagnetization curves for $Nd_{15.78}Fe_{76.3-x}Hf_{0.2}B_{7.8}$ ($x = 0.2$) submitted to solid-HD at 800 °C followed to DR at 850 °C. Solid lines stand for the result of the fitting procedure using formula (2).

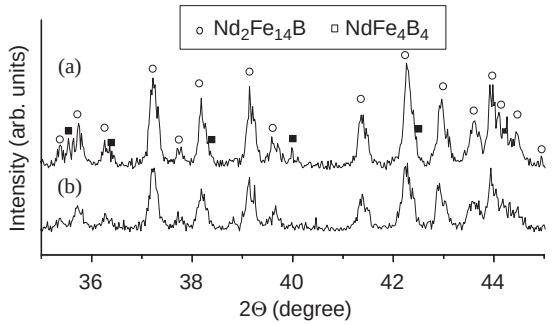

Fig. 5. X-ray diffraction patterns of Hf ($x = 0.2$) added samples submitted to (a) C-HDDR 900 °C and (b) S-HDDR 850 °C.

fitting procedure of the demagnetization curve are listed in Table 1 (as an example to show the goodness of the fit see Fig. 4).

No significative differences appear neither in the XRD difractograms (see Fig. 5, only results of Hf-added alloys C-HDDR treated at 900 °C and solid-HDDR treated at 850 °C are shown as an example) nor ME spectra obtained from all the samples (Fig. 6), all the spectra being well fitted with a set of six sextets and a doublet corresponding to 95% and 5% of ^{57}Fe atoms in $Nd_2Fe_{14}B$ and in $Nd_1Fe_4B_4$, respectively; no other magnetic phases besides $Nd_2Fe_{14}B$ are present in our samples in detectable amounts.

The apparent features of EXAFS oscillations for Hf-added alloys, as-cast and submitted to different HDDR processes are all similar as shown in Fig. 7. This result suggests that local structure or short range order (configuration including first and at most second neighbours) around Hf atoms is the same in all the samples. The unit cell of $Nd_2Fe_{14}B$ ($P4_2/mmm$ space group) [12] consists of 68 atoms where Nd occupies two inequivalent sites (4f and 4g), Fe occupies six inequivalent sites ($16k_1$, $16k_2$, $8j_1$, $8j_2$, 4e and 4c) and B occupies one site (4g). Calculations of $k\chi(k)$ for Hf substituting one of any Nd or Fe sites were carried out using FEFF7. Fig. 8 shows these results together with the observed signal for solid-HDDR treated at

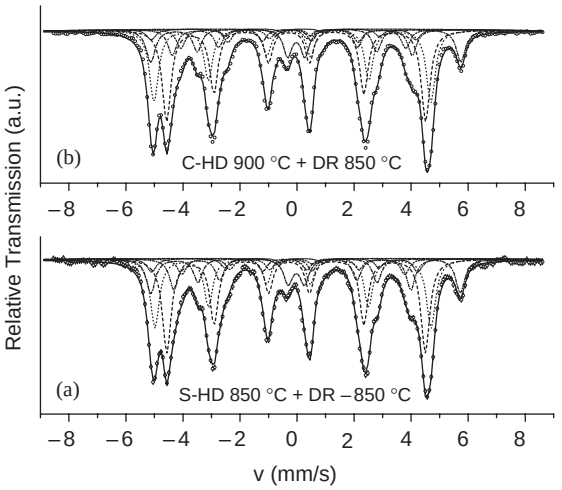

Fig. 6. Mössbauer effect spectra of $Nd_{15.78}Fe_{76.3-x}Hf_{0.2}B_{7.8}$ ($x = 0.2$) submitted to solid (a) and conventional (b) HDDR treatment.

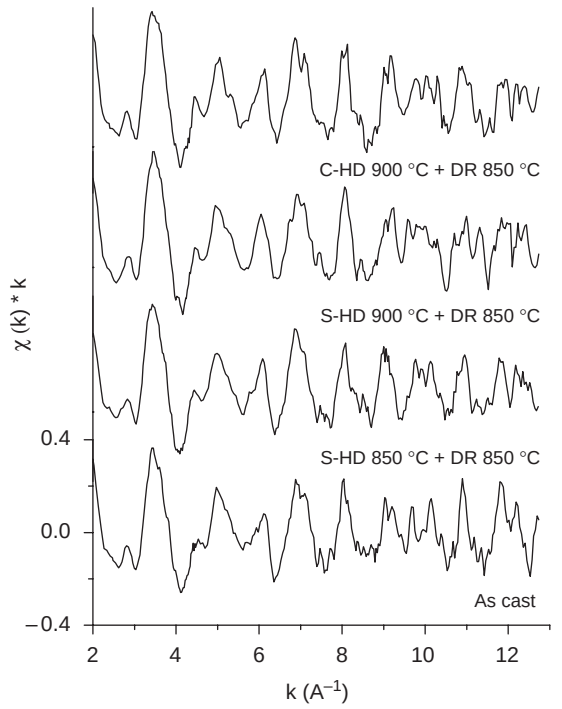

Fig. 7. Observed EXAFS results at Hf L_{III} edge for as-cast $Nd_{15.78}Fe_{76.3-x}Hf_{0.2}B_{7.8}$ ($x = 0.2$) and submitted to various HDDR treatments.

850 °C sample. No match between these oscillations and the experimental one was obtained by locating Hf neither in any of these sites nor in any

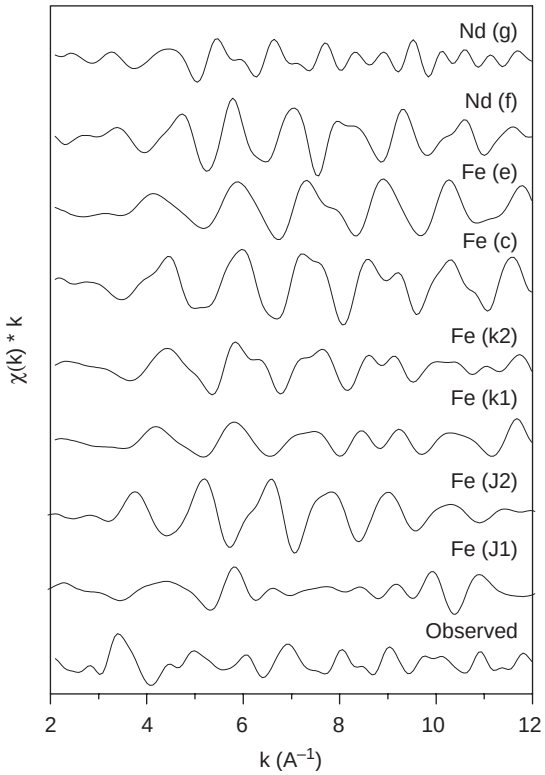

Fig. 8. Calculated $k\chi(k)$ results using FEFF 7 for Hf L-edge with Hf substituting one of the six Fe-sites and two Nd-sites in the $Nd_2Fe_{14}B$ structure. The observed signal is shown at the bottom.

site of the HfB_2 (see top of Fig. 9), orthorhombic HfB (space group Pnma), Hf–Fe or $Nd_1Fe_4B_4$ structures. However, the experimental oscillation matches very well with the FEFF calculated one (see Fig. 9, bottom left) for cubic HfB (ClNa-type, space group Fm3m) [13]. Fig. 9 (bottom right) represents the Fourier transformation (FT) of the calculated $k\chi(k)$ signal (for Hf in HfB) along with the observed one for the same k-range, i.e. 3.1–10 $Å^{-1}$. Note that in this figure, the scales of both FT were chosen in order to facilitate the visual comparison. The FT amplitude of the FEFF signal is larger than the measured one due to the fact that in the FEFF calculation true damping parameters were not introduced. The coincidence between them is good concerning the first three neighbour layers positions and their relative amplitudes.

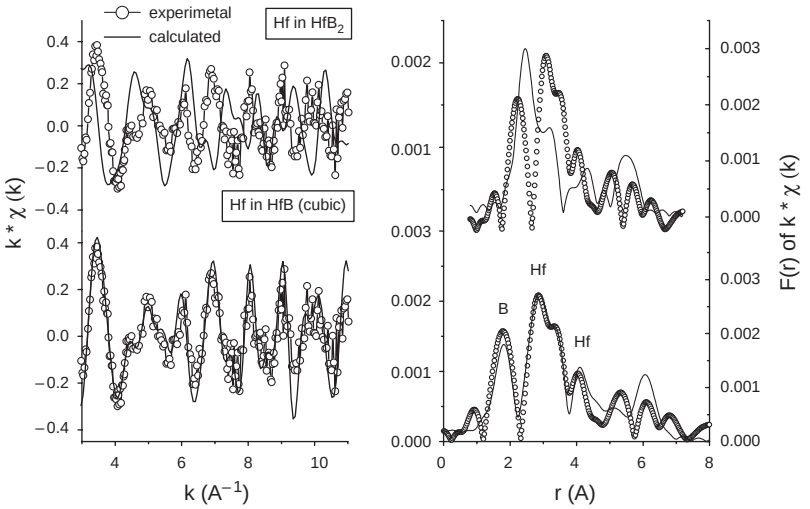

Fig. 9. Left: Comparison between observed XAFS spectra and calculated results obtained by locating Hf in Hf_2B (top) and HfB (bottom) structure. Right: FTs of $k\chi(k)$ of the spectra shown on the left, dots stand for FT of the experimental signal and solid line for FEFF calculated ones. The left scale correspond to the observed signal FT and the right scale to the calculated one.

4. Discussion

Hf-doped alloys treated under S-HDDR at 800 and 850 °C exhibit a significant degree of anisotropy. The inflection registered in the demagnetization curve corresponding to these samples and the increase of remanence (see Fig. 1) is characteristic of nanocomposite materials consistent of a mixture of hard and soft magnetic grains, like $Nd_2Fe_{14}B$/Fe composites (situation which has been observed for Nd deficient samples) [14]. However, this is not our case since neither free iron nor other magnetic phases (besides $Nd_2Fe_{14}B$) were detected in our samples (see ME spectra in Fig. 6). The reason for this hard–soft-type behaviour could be attributed to microstructural differences within the same material. If a non-homogeneous distribution of grain sizes have occurred, leading to the coexistence of relatively small single-domain grains and larger multi-domain ones, the former would show a harder behaviour than the latter, where domain wall motion would easily occur in the absence of important sources of pinning. The occurrence of large grains could be a consequence of abnormal grain growth or of incomplete disproportionation. This last possibility is excluded due to the following fact: previous tests of the used experimental set up (reactor pressure and temperatures, material amount, powder size, etc.) indicate that the time needed to achieve complete disproportionation is much shorter than 100 min, i.e. for a ternary alloy 15 min is enough. As mentioned in the previous section the anisotropic component is the softer one (Fig. 2), Hf alloys anisotropy would then originate, within our interpretation, in the large, abnormally grown grains. One possible reason for this is that large grains were capable to become preferentially oriented during the cold compactation process under a 2 T magnetic field. Small ones, of which there are many and randomly oriented within each powder particle, would not be able to undergo this process.

Formation of cubic HfB (Fm3m) in the as-cast and in the HDDR treated samples is inferred from EXAFS calculation. HfB phase with the ClNa-type structure only has been reported as an impurity stabilized phase [15] and not as a metastable pure phase. This structure type is the equilibrium one for HfN, which is known [16] to form, starting from hexagonal Hf structure, by adding N atoms to the octahedral interstices. At a given N concentration the lattice transforms to cubic HfN (ClNa-type). It is possible that boron atoms from grain boundary diffuse into metallic Hf inducing a similar lattice transformation.

The present results indicate that Hf addition has a noticeable effect on the magnetic properties of S-HDDR processed samples and these clearly show that Hf is not in the $Nd_2Fe_{14}B$ structure but incorporated into a local structure (cubic-HfB type) which is the same for all of our samples; such magnetic behaviour would then be related to microstructural features.

5. Summary and conclusions

EXAFS results clearly show that Hf is not in the $Nd_2Fe_{14}B$ structure but incorporated into a local structure (HfB ClNa-type) which is the same for all of our samples. However, it was observed that only Hf added solid HDDR $Nd_{16}Fe_{76}B_8$ materials exhibit significant degree of anisotropy. The anisotropic samples present a behaviour characteristic of a mixture of two magnetic component materials (one component hard and the other soft). A fitting function was proposed to analyse the demagnetization curves which allow the retrieval of information of the remanent polarizations, coercivity fields and relative fractions of both components. The hard–soft behaviour can be explained under the assumption that there is a non-uniform distribution of $Nd_2Fe_{14}B$ grain sizes in some of our samples. Within this hypothesis the soft component is assigned to partially oriented multidomain large grains of $Nd_2Fe_{14}B$ while the other one arises form single-domain grains of the same phase.

Acknowledgements

This research was supported by CONICET and CICPBA of República Argentina and partially supported by LNLS through the Programa de Auxilio. We are indebted with the LNLS XAS1 beam line staff for help with XAFS experiment and with Dr. O. Gutfleisch for the use of the IFW laboratory facilities.

References

[1] R. Nakayama, T. Takeshita, J. Alloys Compounds 193 (1993) 259.
[2] P.J. McGuiness, S. Kobe, I. Skulj, A. Bollero, O. Gutfleisch, E.J. Devlin, D. Niarchos, J. Magn. Magn. Mater. 237 (2001) 267.
[3] T. Tomida, N. Sano, K. Hanafusa, H. Tomizawa, S. Hirosawa, Acta Mater. 47 (1999) 875.
[4] M. Uhehara, P. Choi, T. Tomida, H. Tomisawa, S. Hirosawa, I. Maehara, IEEE Trans. Magn. 31 (1996) 4368.
[5] A. Ashfaq, M. Matsuura, M. Sakurai, J. Magn. Magn. Mater. 212 (2000) 368.
[6] P. deRango, F.N. Genin, D. Fruchart, A. Traverse, S. Rivoirard, I. Popa, J. Magn. Magn. Mater. 226–230 (2001) 1377.
[7] T.W. Capehart, R.K. Mishra, F. Pinkerton, J. Appl. Phys. 10 (1993) 6476.
[8] T. Ressler, J. Phys. IV (7) (1997) C2–269.
[9] A.L. Ankoudinov, J.J. Rehr, Phys. Rev. B 56 (1997) R1712.
[10] J.C. Cezar, H.C.N. Tolentino, L. Knobel, J. Magn. Magn. Mater. 233 (2001) 103.
[11] J.M.D. Coey (Ed.), Rare-earth Iron Permanent Magnets, Clarendon Press, Oxford, 1996 p. 62.
[12] J.F. Herbst, J.J. Croat, F.E. Pinkerton, Phys. Rev. B 29 (1984) 4176.
[13] T.B. Massalski (Ed.), Binary Alloy Phase Diagrams, second ed., ASM International, 1990, p. 448.
[14] O. Gutfleish, J. Phys. D 33 (2000) R157.
[15] F.W. Glaser, D. Moskpwitz, B. Post, Trans. AIME 197 (1953) 1119.
[16] M.A. Bab, L. Mendoza Zélis, L.C. Damonte, Acta Mater. 49 (2001) 4205.